RSC Advances

PAPER

View Article Online
View Journal | View Issue

Cite this: *RSC Adv.*, 2017, **7**, 8303

Enhancing the performance of SPEEK polymer electrolyte membranes using functionalized TiO_2 nanoparticles with proton hopping sites

Parisa Salarizadeh,[ab] Mehran Javanbakht*[ab] and Saeed Pourmahdian[c]

In this work, the application of a sulfonated poly(ether ether ketone) (SPEEK)/amine functionalized titanium dioxide nanoparticle (AFT) composite as a novel membrane in proton exchange membrane fuel cells (PEMFC) was studied. Titanium dioxide (TiO_2) nanoparticles were functionalized by grafting aminopropyl groups through hydrolysis of 3-aminopropyltriethoxysilane (APTES). The influence of the AFT nanoparticles on thermal and mechanical stability, water uptake, dimensional stability and electrochemical properties of the membranes were studied. The grafting of APTES onto TiO_2 nanoparticles improved their dispersion in the SPEEK matrix. The nanocomposite membrane with the optimal amount of AFT nanoparticles, 7.5 wt%, showed a proton conductivity of 0.135 S cm^{-1} at 80 °C which was 159.6% higher than that of the nanocomposite membrane with 7.5% TiO_2. This can be attributed to their good dispersion and reduction of interparticle separation spacing which creates connected pathways for proton transport. The membrane with 7.5 wt% AFT showed a 40.8% decrease in swelling, a 132.7% increase in conductivity and an 86.7% increment in maximum power density (PD_{max}) (230 mW cm^{-2}) compared with the pristine SPEEK membrane, which indicated its potential application in PEMFCs.

Received 28th October 2016
Accepted 16th January 2017

DOI: 10.1039/c6ra25959f

www.rsc.org/advances

1. Introduction

Proton exchange membrane fuel cells (PEMFCs) are electrochemical devices that generate electricity, water and heat by a simple reaction between hydrogen and oxygen gases. PEMFCs have received much consideration because of their wide applicability, high efficiency, low pollution and quick start time.[1–3] A proton exchange membrane (PEM) is the key component in the development of PEMFCs. The commercial membrane used in PEMFCs is Nafion due to its good proton conductivity at temperatures below 80 °C, and high chemical and oxidative stability.[4] But, Nafion has its own inherent drawbacks such as high cost, limited operation temperature and fuel crossover.[5] Synthesizing novel PEMs with excellent proton conductivity, low cost, good thermal and mechanical stability and high fuel cell performance is essential for the development of PEMFCs.[6] Our earlier literature reported on the synthesis of nanocomposite membranes by incorporating some inorganic nanoparticles as filler such as, SBA-15-ph-SO_3H,[7] poly(sulfonic acid)-*g*-silica,[8] $BaZrO_3$,[9] $La_2Ce_2O_7$,[10] sulfonated graphene oxide (SGO),[11,12] and Fe_2TiO_5 nanoparticles[13] for enhancing the mechanical stability, the proton conductivity and other properties of membranes.

Sulfonated poly(ether ether ketone) (SPEEK) is a non-fluorinated polymer considered as a reliable candidate for PEM application due to its high thermo-oxidative resistance, superior chemical stability, good thermal stability and low cost.[14] Increase in sulfonation degree (DS) of SPEEK increases the membrane swelling and proton conductivity and declines the membranes mechanical stability because of the plasticizing nature of sulfonated groups.[15,16] The DS of SPEEK can easily be controlled by the reaction time, concentration of acid and temperature.[17] Different approaches have been investigated to improve various properties of SPEEK such as, mechanical properties, dimensional stability and proton conductivity, including blending with other polymers,[18] cross-linking[19] and addition of inorganic fillers.[17,20]

Inorganic hygroscopic nanofillers such as titanium dioxide (TiO_2), zirconium oxide (ZrO_2), silica (SiO_2) and iron titanate (Fe_2TiO_5) nanoparticles[21–24] have been added to SPEEK membranes to further enhance physicochemical properties with suitable electrochemical properties. But, usually with the adding of the inorganic nano-fillers, the proton conductivity of the membranes declines due to the tendency of fillers to agglomeration, their low compatibility with polymer matrix and dilution effect on sulfonic acid sites in the SPEEK matrix.[25] To overcome these problems, surface treatment of nanofillers with

[a]*Department of Chemistry, Amirkabir University of Technology, Tehran, 1599637111, Iran. E-mail: mehranjavanbakht@gmail.com; Fax: +98 21 64542762; Tel: +98 21 64542764*

[b]*Fuel Cell and Solar Cell Laboratory, Renewable Energy Research Center, Amirkabir University of Technology, Tehran, 1599637111, Iran*

[c]*Department of Polymer Engineering and Color Technology, Amirkabir University of Technology, Tehran, 1599637111, Iran*

acidic and basic organic groups can be an effective method.[25–29] Moreover, the modification of the nanoparticles with these functional groups can form proton hopping sites for Grotthuss-type proton transfer, as a result, the proton conductivity of the membrane improves.[26]

In our previous work, incorporation of modified Fe_2TiO_5 nanoparticles within SPEEK matrix improved proton conductivity and mechanical properties of membrane.[30] Our research was continued with investigation of different nanoparticles effect and their surface modification on the properties of nanocomposite membranes. P25 TiO_2 nanoparticles have high hydroxyl groups in their surface which facilitate its surface modifications. Many researchers confirmed bio-catalytic properties of amine functionalized TiO_2 nanoparticles for waste water treatment[31,32] but it is less studied as a nanoparticle with proton hopping sites in PEMFC. In present work, a novel SPEEK/amine functionalized TiO_2 nanocomposite membrane was prepared with the aim of enhancing proton conductivity and physicochemical properties of SPEEK-based membranes. The thermal and mechanical stability, water uptake, membrane swelling, ion exchange capacity (IEC), proton conductivity and PEMFC performance of the membranes were evaluated. $-NH_2$ groups of functionalized TiO_2 nanoparticles provided hydrogen bonding and electrostatic interactions with $-SO_3H$ groups of the polymer matrix which created further proton transfer sites and increased the proton conductivity of the membranes. Moreover, the modification of TiO_2 nanoparticles diminished their agglomeration and improved the proton conductivity of membranes by creating continues pathways for proton transport.

2. Experimental

2.1. Materials

Poly(ether ether ketone), PEEK, (MW = 20 800) was supplied from Sigma-Aldrich. P25 TiO_2 nanoparticles with particle size of 21 nm, specific surface area of 50 ± 15 $m^2\ g^{-1}$ was purchased from Degussa. Triethyl amine (TEA) and 3-amino-propyltriethoxysilane, APTES, were purchased from Merck. All of the solvents were obtained from Merck. De-ionized water was used throughout the experiments.

2.2. Synthesis of amine functionalized TiO_2 nanoparticles and SPEEK

Amine functionalized TiO_2 (AFT) nanoparticles were prepared by the two-step method as illustrated in Fig. 1 according to the following procedure: first, 1 g of TiO_2 nanoparticles was dried at 100 °C in a vacuum oven, and then dispersed in 100 mL anhydrous toluene. Then, 8 mL of APTES and 0.6 mL of triethyl amine were added drop by drop to the resulting solution and refluxed under N_2 atmosphere for 24 h at 80 °C. At the end, the

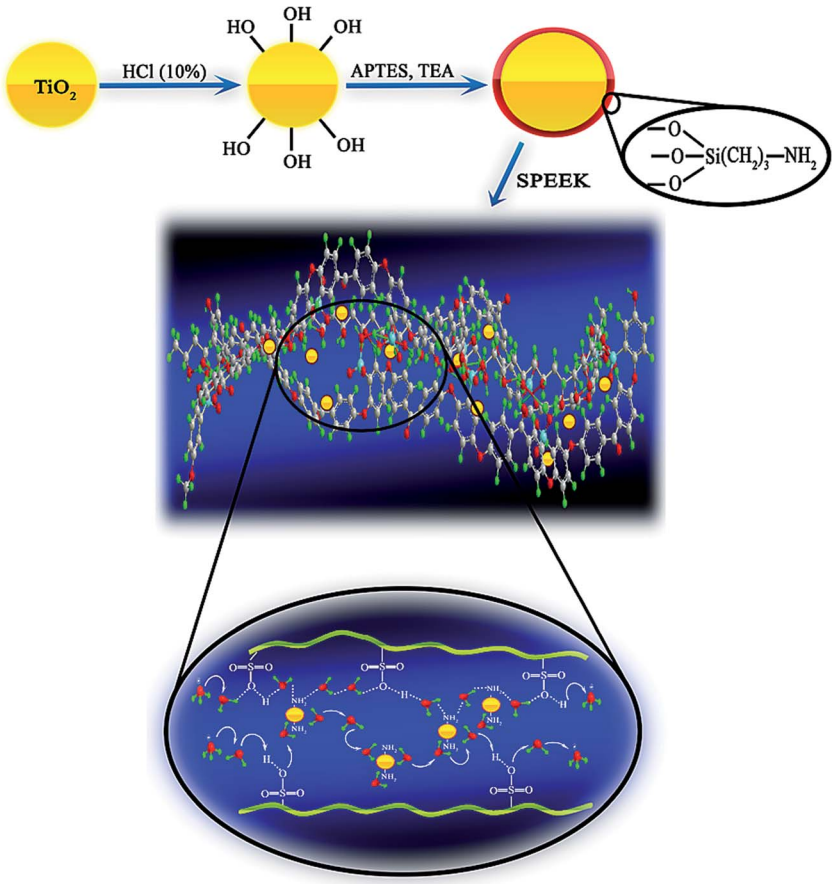

Fig. 1 Schematic of amine-functionalization reaction of TiO_2 nanoparticles and the proton transfer mechanism in the nanocomposite membrane.

resulting mixture was washed three times with toluene and ethanol, respectively and dried in a vacuum oven.

Sulfonated poly(ether ether ketone) (SPEEK) was prepared by direct sulfonation of PEEK. First, dried PEEK (10 g) was dissolved into concentrated sulfuric acid (100 mL) under stirring at 25 °C for 1 h. Then, the polymer solution was stirred for 4 h at 60 °C under nitrogen atmosphere. The sulfonated polymer solution was cooled and then precipitated in excess amount of ice-water under continuous stirring. The solid SPEEK was washed with deionized water till neutral pH and then dried at 70 °C for 24 h. The DS was found to be 68% by titration method.

2.3. Membrane preparation

Three types of membranes (SPEEK, SPEEK/TiO_2 and SPEEK/AFT) were synthesized by the solution casting method; these membranes were identified as SP, SP_{Tx} and SP_{AFTx} respectively, where x (2.5, 5, 7.5 and 10) represents the weight percentage of nanoparticles in the nanocomposite membranes. At first, 1 g of SPEEK was dissolved in 3 mL of DMAc by stirring at room temperature for 1 h. Then, the appropriate weight of nanoparticles was dispersed in 2 mL DMAc by sonication for 30 min and then added into the SPEEK solution. The solution was sonicated for 30 min until the mixture became homogeneous. The resultant viscous polymer solution was poured on a clean glass plate by using an automatic film applicator. The membranes were dried at room temperature for overnight and 70 °C for 24 h, respectively. The thickness of the dried resulting membranes was about 70 μm. Among SP_{Tx} membranes, the SP_{T5} membrane selected for more analyze to compare with SP_{AFTx} due to its higher proton conductivity than other SP_{Tx} membranes. Before of all tests, the membranes were treated in 2 M sulfuric acid solution and deionized water, respectively. This was done in order to liberate the residual solvent.

2.4. Characterization

The chemical structures of modified nanoparticles and membranes were characterized by Fourier transform infrared spectrometer (FTIR, Bruker Equinox) in the range of 500–4000 cm^{-1}. The morphology and size of the obtained nanoparticles and cross-sectional morphology of the membranes were investigated by a field emission scanning electron microscope (FESEM, TESCAN). Transmission electron microscopy (TEM, Zeiss EM10C) was used to investigate the size and morphology of the AFT nanoparticles.

The surface topography and roughness of the membranes were evaluated by atomic force microscopy (AFM) technique in tapping mode using a SPA-300HV, Seiko Instrument Co. The X-ray diffraction (XRD) of the prepared membranes was performed using an INEL model EQUINOX 3000, France X-ray diffractometer in an angular range of 5–80°.

The thermogravimetric analysis (TGA) of the nanoparticles and membranes was performed using a Hi-Res TGA 2950 thermogravimetric analyzer under nitrogen atmosphere at the heating rate of 10 °C min^{-1}. The mechanical properties of the membranes were evaluated on a STM-150 universal test machine (UTM, SANTAM DBBP, Iran) with an elongation rate of 2 mm min^{-1}.

2.5. Water uptake and membrane swelling

At first, the nanocomposite membranes were immersed in deionized water at room temperature for 12 h until fully hydrated. After wiping the surface water of membranes, the weight (W_w) and length (L_w) of membranes were determined. The membranes were then dried at 60 °C for 12 h and dry weight (W_d) and the length (L_d) of the membranes were measured. The membrane swelling (MS) and water uptake (WU) of the membranes were calculated as follows:

$$\mathrm{WU}(\%) = \frac{W_w - W_d}{W_d} \times 100 \quad (1)$$

$$\mathrm{MS}(\%) = \frac{L_w - L_d}{L_d} \times 100 \quad (2)$$

2.6. Proton conductivity and ion-exchange capacity

The proton conductivity of membranes was measured by a four probe technique using an Autolab potentiostat/galvanostat taken between 0.1 Hz and 10^6 Hz at a voltage amplitude of 0.05 V. Before the test, the prepared membranes were soaked in 2 M sulfuric acid solution and deionized water, respectively. Four probe conductivity measurements was performed by a conductivity cell composed of two platinum wires sensing the potential drop, two platinum plates carrying the current and the proton conductivity was obtained as follows:

$$\sigma = \frac{L}{RWT} \quad (3)$$

where L, R, W and T are distance between electrodes (cm), ionic resistance of membrane (Ω), width and the membrane thickness (cm), respectively. Ionic resistance of the membrane, which is ohmic (high frequency) resistance, was determined from impedance spectrum.

The IEC of SP_{AFTx} membranes was measured by the back-titration method.[33] The membranes were immersed into a 2 M sulfuric acid solution for 12 h to ensure that all the Na^+ ions were exchanged with H^+ ions. Then the samples were soaked in deionized water until neutral pH was obtained and dried in an oven. The dried membrane was immersed into 1 M NaCl solution for 24 h and this solution was titrated with 0.01 M NaOH solution. The IEC of the membranes was calculated as follows:

$$\mathrm{IEC} = \frac{MV}{m} \quad (4)$$

where M (mol L^{-1}) is the molar concentration of NaOH solution, V (mL) is the volume of added NaOH at the equivalent point, and m (g) is the dry weight of the membrane.

2.7. Membrane-electrode assembly (MEA) preparation and performance test

For single-cell testing, the anode and cathode electrodes were made by the coating of catalyst ink (including the Pt/C catalyst

(20 wt% of Pt), 5 wt% Nafion solution, isopropyl alcohol, the suitable amount of water and glycerol) onto gas diffusion layer (carbon cloth, E-tek, HT 2500-W) by painting method. The electrodes were dried at 80 °C for 40 min and at 120 °C for 1 h, respectively. The Pt loading 0.25 mg cm^{-2} was kept for both anode and cathode electrodes. For preparation of MEA, two electrodes were located onto both side of the membrane and then hot pressed under 135 kg cm^{-2} pressure at 120 °C for 3 min. The PEMFC performances were measured at different temperatures using the FCT 1505 fuel cell test system. The H_2 and O_2 input flow rates were 120 and 300 mL min^{-1}, respectively.

3. Results and discussion

3.1. Synthesis and characterization of amine functionalized TiO_2

Chemical structure of AFT nanoparticles was verified by FTIR spectroscopy (Fig. 2d). The peaks below 700 cm^{-1} were assigned to the stretching vibration of Ti–O and Ti–O–Ti groups in titania nanoparticles. The broad absorption peak at 3428 cm^{-1} and the low intensity peak at 1621 cm^{-1} in TiO_2 spectra were ascribed to the O–H stretching vibration and bending vibration modes of adsorbed water as well as hydroxyl groups, respectively.[34] The symmetrical and asymmetrical vibrations of $-CH_2$ groups and also the bending vibration of C–H groups were observed at 2854, 2923 and 1461 cm^{-1}. Furthermore, the stretching vibration of Si–O–Si groups at 1030 and 1130 cm^{-1} was observed in the spectrum of the AFT nanoparticles.[35,36] The peak at 940 cm^{-1} is allocated to Ti–O–Si vibration.[34,37] These bands confirmed the successful surface modification of the TiO_2 nanoparticles with silane coupling agent.

Also, TGA was utilized to illustrate the successful surface modification of the TiO_2 with APTES. The TGA and differential TGA (dTGA) curves are shown in Fig. 2e. The amount of APTES grafted on the surface of TiO_2 was estimated from the resultant curve and obtained at least 9.2%. The weight loss of the bare TiO_2 nanoparticles was attributed to desorption of adsorbed water and dehydration of the hydroxyl groups.[38] AFT nanoparticles exhibited two-step degradation in the temperature between 50–550 °C. The first step at the temperature range of 50–200 °C is assigned to the evaporation of adsorbed water and further condensation of APTES.[39] The second step at the temperature range of 250–600 °C was attributed to degradation of the aminopropyl groups from the nanoparticles surface. The boiling temperature of APTES, 217 °C, is lower than the degradation temperature of APTES grafted on TiO_2 nanoparticles. Hence, it can be assumed that there was chemical bonding between the TiO_2 nanoparticles and APTES.

The morphological features of TiO_2 and AFT nanoparticles were observed by the SEM and TEM images as shown in Fig. 2. It can be seen from Fig. 2a and b that TiO_2 nanoparticles were agglomerated while AFT nanoparticles were dispersed well. This comparison indicates that the APTES plays a key role in the improvement of the interfacial interaction between nanoparticles. Fig. 2c is the TEM image of AFT nanoparticles. It was found that modified nanoparticles were discrete and agglomeration decreased effectively due to the attraction between the particles was decreased.

3.2. Characterization of membranes

ATR spectra of representative membranes, SP, SP_{T5} and $SP_{AFT7.5}$, are displayed in Fig. 3.

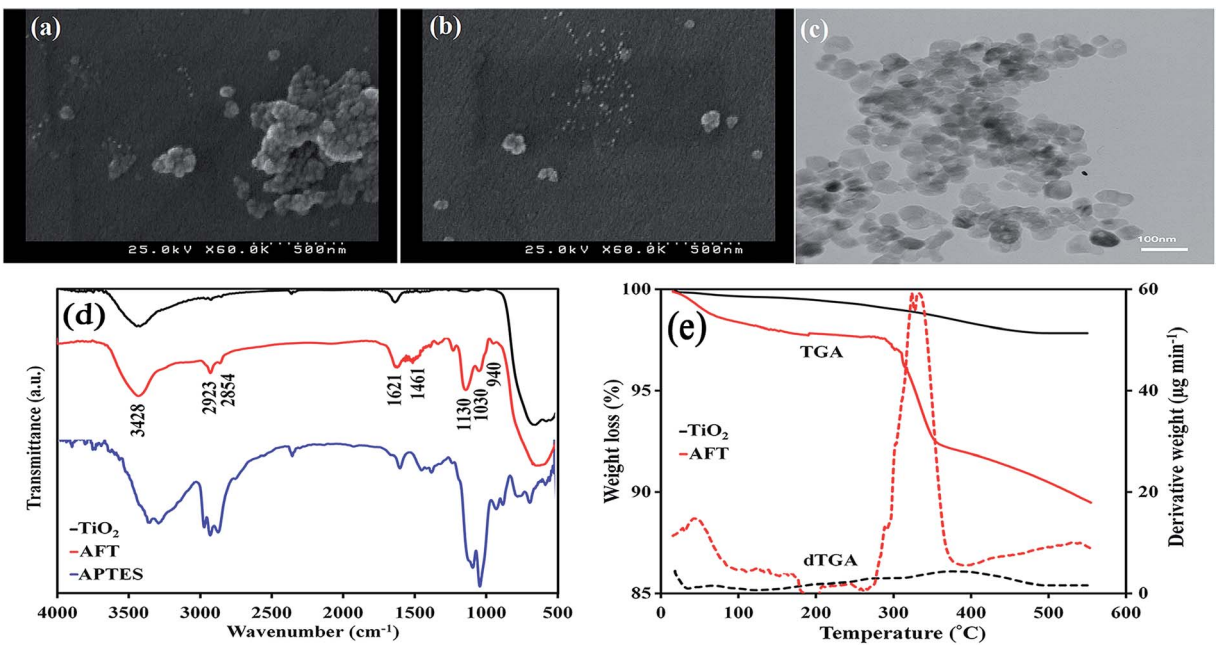

Fig. 2 SEM images of TiO_2 (a) and AFT (b), TEM image of AFT nanoparticles (c), FTIR spectra of TiO_2, AFT and APTES (d) and TGA curves and corresponding dTGA curves of nanoparticles (e).

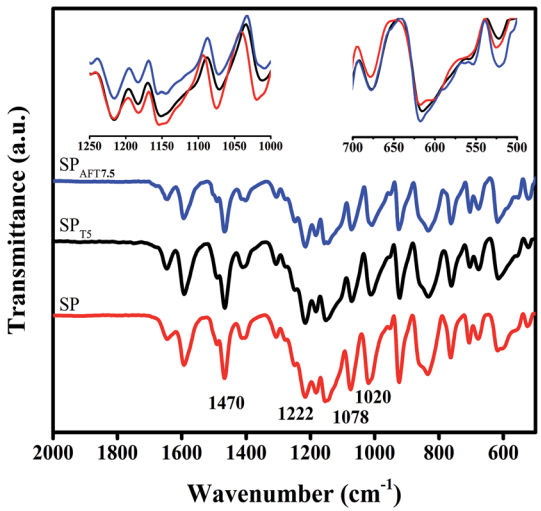

Fig. 3 ATR spectra of SP, SP_{T5} and $SP_{AFT7.5}$ membranes.

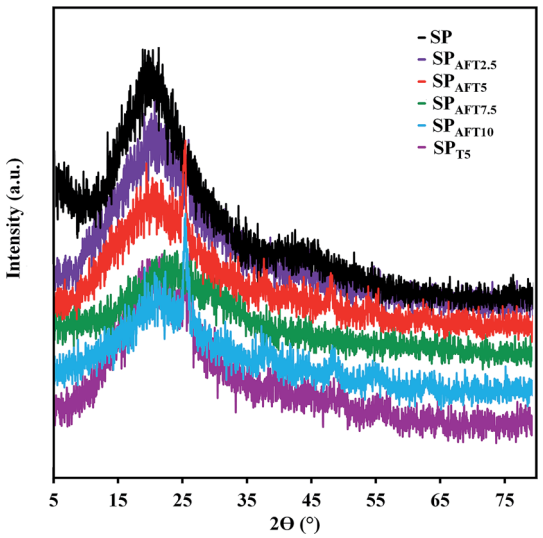

Fig. 4 X-ray diffraction patterns of the SP and nanocomposite membranes.

The successful sulfonation of PEEK backbone was verified by observing characteristic peaks at 1020, 1078 and 1222 cm^{-1}, corresponding to the symmetric and asymmetric stretching vibrations of sulfonic acid groups.[26] The intensity of these peaks in SP_{T5} and $SP_{AFT7.5}$ membranes were found relatively lower, which indicated the interaction between SO_3H groups and functional groups of nanoparticles.[25] The peaks at 1470 and 1490 cm^{-1} were attributed to C=C stretching vibration of the aromatic rings.[3] After incorporating TiO_2 and AFT nanoparticles into membranes, the intensity of the peaks at range of 550–700 cm^{-1} slightly increased likely due to overlapping TiO_2 absorption peak (Ti–O–Ti) with the polymer peaks and the increase was more evident in $SP_{AFT7.5}$ than SP_{T5}.

SPEEK and nanocomposite membranes were characterized by XRD to investigate the structural changes resulting from incorporation of AFT and TiO_2 nanoparticles. XRD patterns of the as-prepared membranes based on AFT nanoparticles are presented in Fig. 4. It is clear that the crystallinity of PEEK decreased after sulfonation because of incorporation of sulfonic acid groups on the polymer chain randomly.[40] SPEEK showed a broad crystalline peak on the 2θ of 18–19°. It can be seen that the peak intensity of the SP_{T5} and SP_{AFTx} membranes was greatly reduced compared with the SP membrane due to the incorporation of nanoparticles which means that the degree of crystallinity is decreased. Also, SP_{AFT5} showed lower crystallinity than SP_{T5} due to better dispersion of these nanoparticles. These results show that more amorphous domains were created in SP_{AFTx} nanocomposite membranes, indicating the AFT nanoparticles were mixed with SPEEK matrix homogeneously and the membrane structure was more disordered. The amorphous structure of nanocomposite membranes is useful for the enhancement of ionic conductivity.[41,42] However, AFT incorporation further (more than 10%) slightly increases the peak intensity likely because the aggregation of nanoparticles.

The crystallinity percentage (X_c) of the SP, SP_{T5} and SP_{AFTx} nanocomposite membranes was calculated by the empirical relation between X_c and β according to eqn (5).[42]

$$\beta \times (X_c)^{1/3} = K_A \quad (5)$$

where, β is the full width of the peak at half intensity in 2 theta degree (FWHM) and K_A is a constant and is assigned 0.24. Table 1 presents the crystallinity percentage of SP, SP_{T5} and SP_{AFTx} membranes. It is obvious that with the addition of AFT nanoparticles up to 7.5 wt%, the crystallinity percentage of SP_{AFTx} membranes diminished. But, AFT further contents led to an increase in the X_c. The amorphous nature of nanocomposite makes it more flexible which is a favorable character for a polymer electrolyte membrane.

3.3. Morphology and surface topography

Cross-section FESEM images of as-prepared membranes are indicated in Fig. 5. All of the membranes were synthesized without obvious structural defects. The AFT nanoparticles were dispersed homogeneously within the membrane compared with TiO_2 nanoparticles with the particle size of about 21 nm. TiO_2 nanoparticles tend to aggregation (Fig. 5d) which was attributed to high surface energy of nanoparticles and low compatibility with polymer matrix. Aggregation of nanoparticles likely created relatively large regions devoid of any nanoparticle in the membrane that disconnected the

Table 1 The percentage crystallinity of the SP and nanocomposite membranes

Membrane	FWHM (Rad.)	Crystallinity (%)
SP	0.1601	3.3687
$SP_{AFT2.5}$	0.2430	0.9634
SP_{AFT5}	0.2469	0.9185
$SP_{AFT7.5}$	0.2611	0.7766
SP_{AFT10}	0.2252	1.2104
SP_{T5}	0.2366	1.0437

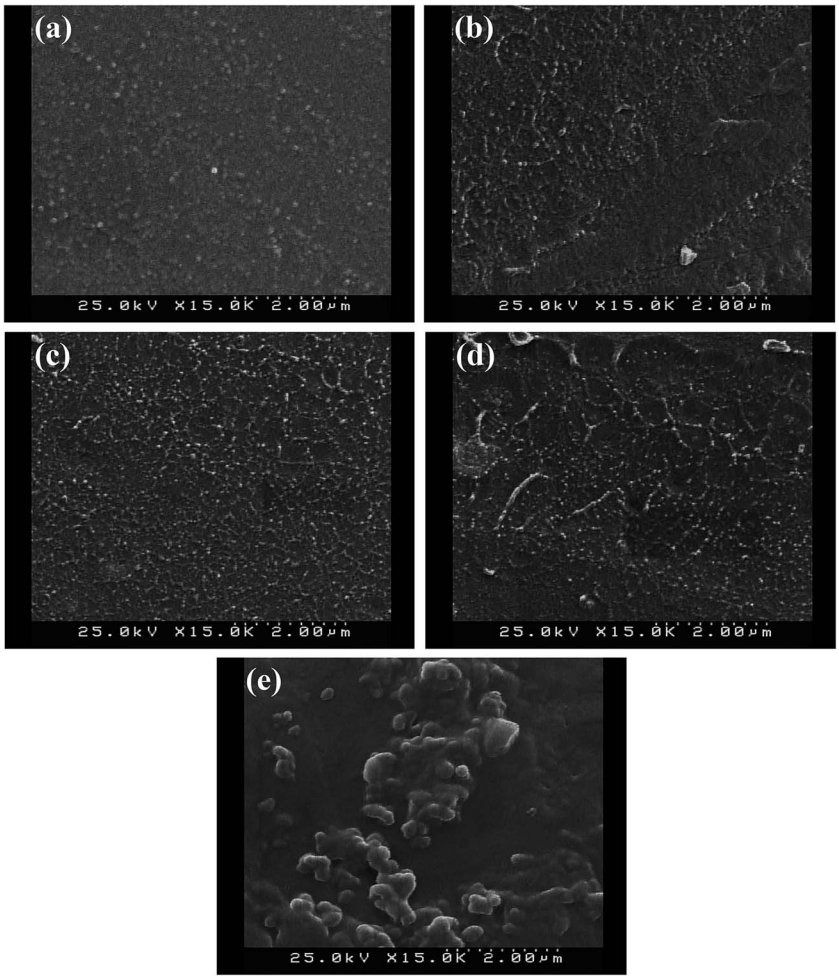

Fig. 5 FESEM images of cross-section of the nanocomposite membranes: $SP_{AFT2.5}$ (a), SP_{AFT5} (b), $SP_{AFT7.5}$ (c) and SP_{AFT10} (d) and SP_{T5} (e).

transportation of the proton in membrane.[25] The grafting of APTES onto TiO_2 nanoparticles caused uniform dispersion of AFT nanoparticles in nanocomposite membranes due to interaction between NH_2 groups of AFT nanoparticles and SO_3H groups of SPEEK matrix. The interfacial compatibility between AFT nanoparticles and polymer matrix is conducive for creation proton transfer continues channels.

Surface roughness is another key factor which has a significant effect on the water uptake and proton conductivity properties of the membranes. Fig. 6 indicates AFM images (2D and 3D) of the SP, SP_{T5} and SP_{AFTx} nanocomposite membranes at a scan size of 5 μm × 5 μm. The bright and dark regions in the images are related to the differences in domain hardness. The bright regions were dedicated to the hydrophobic polymer backbone and the dark regions were ascribed to a soft structure, which represent the hydrophilic sulfonic acid groups.[43] From Fig. 6, the surface topography of the prepared membranes changed considerably after incorporation of nanoparticles. The roughness average (R_a) of SP was 4.06 nm, whereas the R_a of $SP_{AFT2.5}$, SP_{AFT5}, $SP_{AFT7.5}$, SP_{AFT10} and SP_{T5} nanocomposite membranes increased to 6.74, 8.59, 10.80, 14.82 and 12.01 nm respectively. The increase of roughness might lead to the improvement in the water uptake and thus the proton conductivity of the membranes due to higher surface area.[43,44]

3.4. Water uptake and membrane swelling

Water uptake and membrane swelling are vital parameters which directly effect on the most of the membrane properties. Fig. 7a displays the water uptake and swelling of SP_{Tx} and SP_{AFTx} membranes at room temperature. The water uptake of the SP_{Tx} and SP_{AFTx} nanocomposite membranes were higher than that of the SP membrane and increased significantly with increasing the nanofiller content in the nanocomposite membranes. This can be ascribed to the water retention character and the hydrophilic nature of TiO_2 nanoparticles. Also, with increasing of AFT content, volume of water channels somewhat increased and the dead end channels interconnected.[45] But, the further increase in the filler contents, more than 5 wt% for TiO_2 and 7.5 wt% for AFT nanoparticles, resulted in a decrease in the water uptake content. It can be assigned to accumulation and the blocking effect of nanoparticles that may prevent from water molecules entrance to polymer matrix. Generally, water uptake of SP_{AFTx} membranes was lower than SP_{Tx} membranes due to slightly lower hydrophilicity of AFT nanoparticles than TiO_2

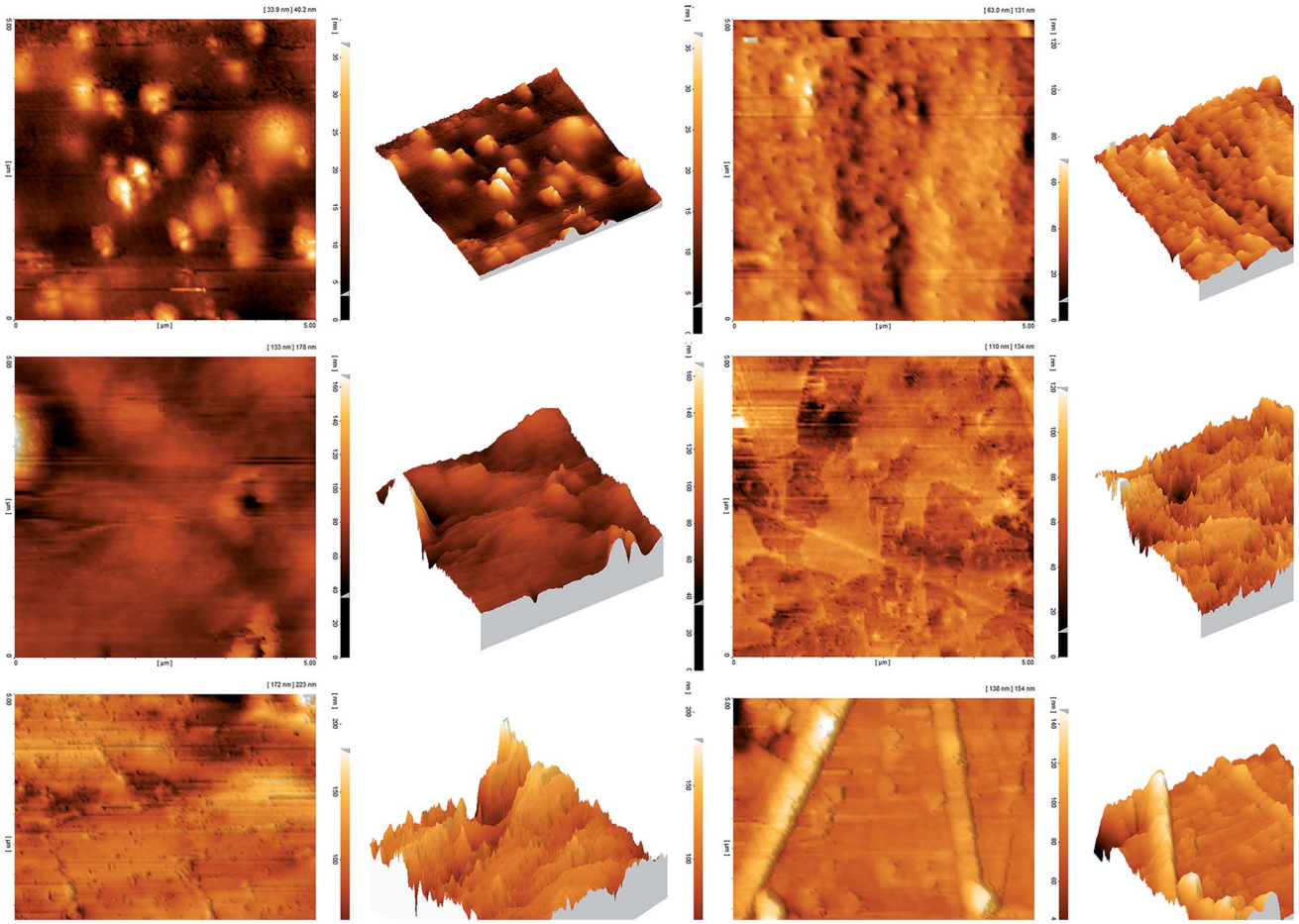

Fig. 6 AFM images (3D and 2D) of SP (a), $SP_{AFT2.5}$ (b), SP_{AFT5} (c), $SP_{AFT7.5}$ (d), SP_{AFT10} (e) and SP_{T5} (f) membranes.

nanoparticles and also the formation of the hydrogen bond between SPEEK chains and AFT nanoparticles. However, at the higher contents of TiO_2 (more than 5 wt%), water uptake of $SP_{T7.5}$ and SP_{T10} membranes were lower than $SP_{AFT7.5}$ and SP_{AFT10} membranes, respectively due to the agglomeration and the blocking effect of nanoparticles.

The high swelling of the membranes lead to low durability, low mechanical stability and so would decrease the fuel cell performance. Generally, reasonable swelling can provide larger space and more continuous pathways for proton transport through the membranes.[25] From Fig. 7a, the membranes swelling in length declined with the addition of TiO_2 and AFT nanoparticles. This result may be from two possible reasons. Firstly, TiO_2 and AFT nanoparticles could interact with polymer matrix through hydrogen bonding and electrostatic force between their surface functional groups and sulfonic acid groups of polymer (–OH/–SO_3H and –NH_2/–SO_3H). Secondly, interaction between polymer chains and nanoparticles limited

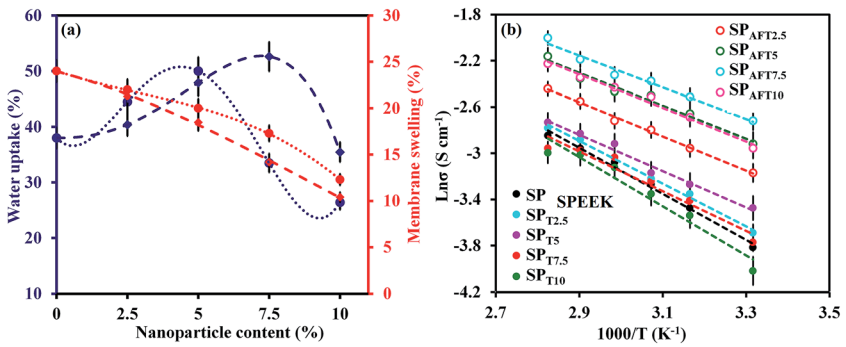

Fig. 7 Water uptake and swelling of SP_{Tx} (dotted line) and SP_{AFTx} membranes (dashed line) at 25 °C (a) and the proton conductivity of nanocomposite membranes as a function of temperatures (b).

the movement of chains in length. Although swelling in length direction was decreased, it was slightly increased in thickness direction. In other words, with addition of fillers, the water uptake and volume swelling were increased. The volume swelling was increased from 27% for SPEEK membrane to 34% and 30% for SP/T5 and SP/AFT7.5 membranes, respectively.

3.5. IEC and proton conductivity

IEC of a membrane indicates the amount of ionizable functional groups in the membrane and expresses as the number of acid groups per one gram of the sample. Normally, the membranes with high IEC value must demonstrate high proton conductivity due to the decrease in the distance between the ionizable groups.[46] IEC values of SP, SP_{Tx} and SP_{AFTx} membranes are given in Table 2. With increasing TiO_2 and AFT nanoparticles contents from 0 to 10 wt%, the IEC values of membranes decreased from 1.95 to 1.79 and 1.77 meq g^{-1}, respectively. The decrease was imputed to the impact of dilution of TiO_2 particles, which lacked the SO_3H groups, and also interaction between polymer SO_3H groups and nanoparticles functional groups.[47,48]

Proton conductivity is a crucial parameter for evaluating the PEMs performance. Proton conductivity of a nanocomposite membrane is influenced by various factors such as IEC, water uptake, dispersion of inorganic fillers and their concentrations in polymer matrix. The proton conductivities of SP and their nanocomposite membranes with different concentration of TiO_2 and AFT nanoparticles in 25 °C are shown in Table 2. Proton conductivity of SPEEK was enhanced with the increment in the amount of TiO_2 and AFT nanoparticles in spite of the IEC value decline. This was ascribed to the hygroscopic properties of nanoparticles, their suitable dispersion in polymer matrix and channeling of water molecules at the interface of the polymer and nanoparticles[49] which created straight transfer pathways for protons and facilitated the proton transfer through the membrane. However, at more than 5 wt% TiO_2 and 7.5 wt% AFT, fillers act as barriers for proton conduction by blocking the proton transfer pathways. The reason may be predomination of dilution effect in higher concentration and the tendency of the TiO_2 nanoparticles to aggregation with increasing the nanoparticle content in the membrane to more than 5 wt%. The SP_{AFTx} membranes demonstrated higher proton conductivity than SP_{Tx}. With increasing amount of TiO_2 and AFT nanoparticles (2.5–10 wt%), proton conductivity improved from 0.087 to 0.105 S cm^{-1} for SP_{AFTx} membranes and decreased from 0.062 to 0.050 S cm^{-1} for SP_{Tx} membranes at 80 °C. Modification of TiO_2 nanoparticles decreased their aggregation and augmented membranes proton conductivities. This is attributed to decrease of interparticle separation spacing which constructs connected proton transfer pathways. Furthermore, $-NH_2$ groups provided the proton hopping sites to proton transfer through Grotthuss mechanism (Fig. 1).

Fig. 7b shows the proton conductivity of SP, SP_{Tx} and SP_{AFTx} membranes at the temperature range of 25–80 °C. In higher temperatures, the proton conductivity enhanced due to increment of the water molecules movement and the mobility increment of the charged species in the membrane.[50,51]

The activation energy (E_a (kJ mol^{-1})) of the proton conduction in the as-prepared membranes was estimated according to Arrhenius equation:

$$\sigma = \sigma_0 \exp(-E_a/RT) \quad (6)$$

where σ and σ_0 are proton conductivity (S cm^{-1}) and pre-exponential factor, respectively. R and T are Boltzmann's constant (J K^{-1} mol^{-1}) and temperature (K), respectively. As revealed from Fig. 7b, the SPEEK membrane displayed the E_a of 15.61 kJ mol^{-1}. The activation energy was obtained 14.48, 12.30, 13.45 and 16.64 kJ mol^{-1} for the $SP_{T2.5}$, SP_{T5}, $SP_{T7.5}$ and SP_{T10} membranes, respectively and 11.55, 11.15, 10.73 and 11.34 kJ mol^{-1} for $SP_{AFT2.5}$, SP_{AFT5}, $SP_{AFT7.5}$, and SP_{AFT10} membranes, respectively. This indicates the easier proton transfer with the increase of AFT and TiO_2 nanoparticles. Also, the SP_{AFTx} and SP_{Tx} membranes showed higher water uptakes than the SP membrane, which might be useful for ionic transport *via* the vehicle mechanism.[52]

A literature review on electrochemical properties of nanocomposite membranes based on some sulfonated polymers and Nafion 117 is demonstrated in Table 3. It is obvious that the electrochemical properties of the $SP_{AFT7.5}$ membrane has improved compared to the other results reported in the literature. This enhancement is ascribed to the good dispersion of modified fillers and channeling of water molecules at the interface of the polymer and fillers which can make continues and straight transfer paths for protons. However, compared to Nafion, the power density of these nanocomposite membranes is yet relatively low, which must be enhanced.

Table 2 Proton conductivity, IEC values and activation energy (in the range of 25–80 °C) of SP and the nanocomposite membranes

	σ (S cm^{-1})			
Membrane	(at 25 °C)	(at 80 °C)	IEC (meq g^{-1})	E_a (kJ mol^{-1})
SP	0.022	0.058	1.95	15.61
$SP_{T2.5}$	0.025	0.062	1.90	14.48
SP_{T5}	0.031	0.065	1.87	12.30
$SP_{T7.5}$	0.023	0.052	1.83	13.45
SP_{T10}	0.018	0.050	1.79	16.64
$SP_{AFT2.5}$	0.042	0.087	1.88	11.55
SP_{AFT5}	0.054	0.115	1.84	11.15
$SP_{AFT7.5}$	0.066	0.132	1.82	10.73
SP_{AFT10}	0.052	0.105	1.77	11.34

3.6. Thermal stability and mechanical properties

Thermal and mechanical properties are vital parameters of PEMs for application in the PEMFCs. The thermal stability of representative membranes, including SP, SP_{T5} and $SP_{AFT7.5}$, were evaluated by the TGA analysis from 50 to 600 °C (Fig. 8). All three membranes demonstrated similar TGA curves comprising of three weight loss stages. The first stage (80–100 °C) was corresponded to the evaporation of residual solvent and physically adsorbed water. The second stage around 300–400 °C was ascribed to the disintegration of SO_3H groups of polymer.[50] The

Table 3 Proton conductivity and PD_{max} of nanocomposite membranes based on some sulfonated polymers and Nafion 117 membrane

Membranes	Filler loading (%)	T (°C)	σ (S cm^{-1})	PD_{max} (mW cm^{-2})	Catalyst loading (mg cm^{-2})	Application	Ref.
SP	0	80	0.058	123	0.25	PEMFC	—
SP_{T5}	5	80	0.065	161	0.25	PEMFC	—
$SP_{AFT7.5}$	7.5	80	0.135	230	0.25	PEMFC	—
SPEEK/SSGO[a]	5	65	0.052	119.6	0.25	PEMFC	2
SPEEK/sMBS[b]	20	80	0.082	—	—	—	53
SPEEK/sMMT[c]	3	60	0.071	19	4	DMFC	54
SPEEK/OMMT[d]	5	90	0.012	—	—	—	55
SPEEK/OMB[b]	15	80	0.079	56	1.3	DMFC	56
SPEEK/IT[e]	2	80	—	188	0.25	PEMFC	24
SPEEK/TNS[f]	1.67	140	0.041	—	—	—	57
SPEEK/MMT[g]	1	25	0.017	—	—	—	58
SPEEK/DSi[h]	9	55	0.033	111.7	0.25	PEMFC	25
SPEEK/TOLP[i]	6	65	0.334	—	—	—	59
SPEEK/TNC[j]	15	25	0.062	—	—	—	26
CSPEEK/HPW[k]/*meso*-SiO_2	20	80	0.12	—	—	—	23
SPEEK/DGO[l]	5	30	0.018	192.1	0.25	PEMFC	60
SPEEK/AIT[m]	2	80	0.12	204	0.25	PEMFC	30
SPI[n]/SPSGO[o]	8	90	0.125	75	5	DMFC	61
SPES[p]/SGO[q]	5	90	0.135	—	—	—	62
Nafion 117	—	80	0.09	—	—	—	63
Recast Nafion	—	80	0.018	640	0.4	PEMFC	3

[a] Sulfonated graphene oxide. [b] Sulfonated mesoporous benzene–silica. [c] Sulfonated montmorillonite. [d] Organic montmorillonite. [e] Iron titanate. [f] Titania nanosheet. [g] Montmorillonite. [h] Dopamine modified silica nanoparticles. [i] Phosphonic acid functionalized titania nanoparticles. [j] Amino acid-functionalized titania nanoparticles. [k] 12-Phosphotungsticacid. [l] Polydopamine modified graphene oxide sheets. [m] Amine functionalized iron titanate. [n] Sulfonated poly imide. [o] Sulfonated propylsilane graphene oxide. [p] Sulfonated poly ether sulfone. [q] Sulfonated grapheme oxide.

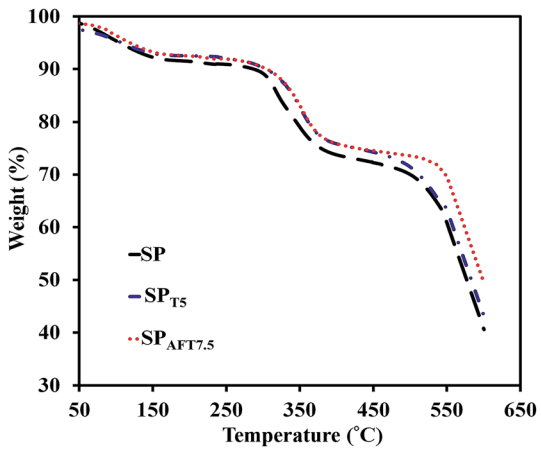

Fig. 8 TGA curves of SP, SP_{T5} and $SP_{AFT7.5}$ membranes.

third stage started from about 450 °C was assigned to the destruction of the polymer backbone. The presence of TiO_2 and AFT nanoparticles slightly delayed the oxidative degradation of polymer matrix and improved thermal stability of the nanocomposite membranes. The nanocomposite membranes showed enough thermal stability up to 300 °C, which are eligible for PEMFCs application.

The mechanical stability of the as-prepared membranes was examined by UTM. Young's modulus (Y_M), tensile strength (T_S) and elongation at break (E_B) of SP_{Tx} and SP_{AFTx} membranes are revealed in Fig. 9. The pure SPEEK indicated Y_M of 700 MPa and T_S of 32.6 MPa. $SP_{T2.5}$ and SP_{T5} membranes illustrated higher T_S and Y_M compared to the SP membrane. With the increase of TiO_2 nanoparticles content (above 5%), T_S and Y_M of nanocomposite membranes decreased because of the aggregation of the TiO_2 nanoparticles in SPEEK matrix. For SP_{AFTx} membranes, with increasing AFT nanoparticles from 2.5–10% both T_S and Y_M increased from 34.6 to 44.3 MPa and 816 to 1391 MPa, respectively. With the modification of TiO_2 nanoparticles, the interaction between AFT nanoparticles and polymer matrix improved and the structure of membranes were more compressed. Also, the homogeneous distribution of modified nanoparticles in the membrane could reduce the repletion of stress in polymer matrix by its transfer to nanoparticles.[8,20] But, E_B of SP_{AFTx} membranes decreased compared with SP membrane, likely due to interaction between NH_2 groups of AFT nanoparticles and SO_3H groups of SPEEK matrix.

3.7. Fuel cell performance

The current density–potential and current density–power density curves of representative membranes, including SP, SP_{T5} and $SP_{AFT7.5}$ nanocomposite membranes in a single cell operating at 80 °C and 90% relative humidity are shown in Fig. 10. SP membrane indicated the maximum current density (I_{max}) of about 515 mA cm^{-2} and the maximum power density (PD_{max}) of 123 mW cm^{-2}. The PEMFC performances of the nanocomposite membranes were enhanced after TiO_2 and AFT incorporation. It was found that incorporating 7.5% AFT caused a 100.6% increase in I_{max} (1033 mA cm^{-2}) and an 86.7% increase in PD_{max} (230 mW cm^{-2}). Compared to AFT, TiO_2 displayed similar effect in enhancing the fuel cell performances of SPEEK-based

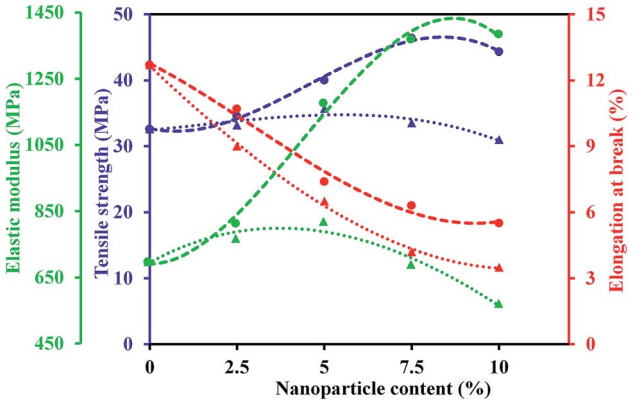

Fig. 9 Mechanical properties of SP_{Tx} (dotted line) and SP_{AFTx} (dashed line) at different content of nanoparticles.

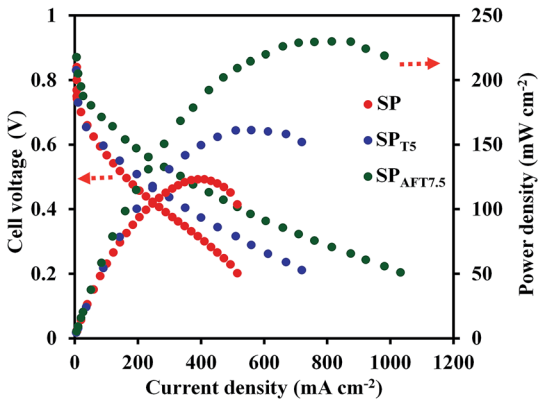

Fig. 10 The current density–potential and current density–power density curves of the SP, SP_{T5} and $SP_{AFT7.5}$ membranes at 80 °C. The H_2 and O_2 flow rates were 120 and 300 mL min^{-1}, respectively.

membrane, and SP_{T5} acquired the I_{max} and PD_{max} of 720 mA cm^{-2} and 161 mW cm^{-2} respectively. This enhancement was attributed to the improved proton conductivities and water uptake of the SP_{T5} and $SP_{AFT7.5}$ membranes compared with pure SPEEK membrane.

4. Conclusion

SPEEK-based membranes were synthesized by embedding TiO_2 and AFT nanoparticles by the solution casting method. Characterization of AFT nanoparticles by FTIR, TGA and TEM demonstrated that TiO_2 nanoparticles were well modified. The influences of AFT nanoparticles on the water uptake, proton conductivity and thermal stability, mechanical properties and PEMFC performance of nanocomposite membranes were investigated. It was observed that by increasing the AFT amount from 0 to 10 wt%, the proton conductivity augmented from 0.058 S cm^{-1} to 0.135 S cm^{-1} at 80 °C due to channeling of water molecules at the interface of the polymer and AFT and the decrease of the interparticle separation spacing which construct connected proton transfer pathways. At the same time, the activation energy results, calculated at the temperature between

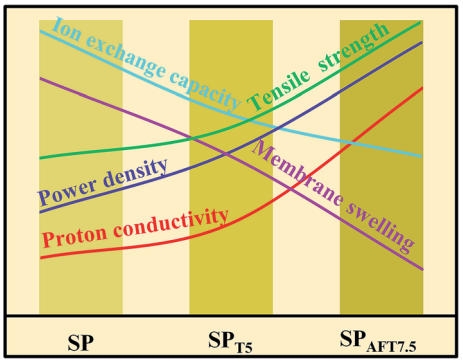

Fig. 11 Effect of TiO_2 and AFT nanoparticles on membrane properties as a function of nanoparticles.

25 and 80 °C, confirmed that the NH_2 groups provided additional sites for proton transfer through Grotthuss mechanism. As a result, SP_{AFTx} membranes showed higher proton conductivity than SP and SP_{Tx} membranes. The $SP_{AFT7.5}$ membrane attained higher PEMFC performance (the current density and power density of 335 mA cm^{-2} and 178 mW cm^{-2} at a cell voltage of 0.5 V at 80 °C, respectively) than SP and SP_{AFTx} membranes at 80 °C due to its higher proton conductivity. The effect of AFT nanoparticles on the properties of the membranes is summarized in Fig. 11. With addition of modified TiO_2 nanoparticles, swelling in length and IEC of membranes was decreased. Also, nanocomposite membrane containing 7.5 wt% AFT nanoparticles showed higher tensile strength, proton conductivity and power density compared with SPEEK and SP/T5 membranes. The excellent proton conductivity and good performance made the SP_{AFTx} membranes attractive candidates for application in PEMFCs.

Acknowledgements

We gratefully acknowledge the financial support from Amirkabir University of Technology (Tehran, Iran), Renewable Energy Research Center (RERC) and Iranian National Science Foundation (INSF).

References

1 V. Kurdakova, E. Quartarone, P. Mustarelli, A. Magistris, E. Caponetti and M. L. Saladino, *J. Power Sources*, 2010, **195**, 7765–7769.
2 L. Zhao, Y. Li, H. Zhang, W. Wu, J. Liu and J. Wang, *J. Power Sources*, 2015, **286**, 445–457.
3 Zh. Di, Q. Xie, H. Li, D. Mao, M. Li, D. Zhou and L. Li, *J. Power Sources*, 2015, **273**, 688–696.
4 A. K. Mohanty, E. A. Mistri, S. Banerjee, H. Komber and B. Voit, *Ind. Eng. Chem. Res.*, 2013, **52**, 2772–2783.
5 A. M. Attaran, M. Javanbakht, K. Hooshyari and M. Enhessari, *Solid State Ionics*, 2015, **269**, 98–105.
6 A. Mayahi, A. F. Ismail, H. Ilbeygi, M. H. D. Othman, M. Ghasemi, M. N. A. M. Norddin and T. Matsuura, *Sep. Purif. Technol.*, 2013, **106**, 72–81.

7 H. Beydaghi, M. Javanbakht, H. Salar Amoli, A. Badiei, Y. Khanianid, M. R. Ganjali, P. Norouzi and M. Abdouss, *Int. J. Hydrogen Energy*, 2011, **36**, 13310–13316.
8 P. Salarizadeh, M. Javanbakht, M. Abdollahi and L. Naji, *Int. J. Hydrogen Energy*, 2013, **38**, 5473–5479.
9 K. Hooshyari, M. Javanbakht, A. Shabanikia and M. Enhessari, *J. Power Sources*, 2015, **276**, 62–72.
10 A. Shabanikia, M. Javanbakht, H. Salar Amoli, K. Hooshyari and M. Enhessari, *J. Electrochem. Soc.*, 2014, **161**, 1403–1408.
11 H. Beydaghi, M. Javanbakht and E. Kowsari, *Ind. Eng. Chem. Res.*, 2014, **53**, 16621–16632.
12 H. Beydaghi and M. Javanbakht, *Ind. Eng. Chem. Res.*, 2015, **54**, 7028–7037.
13 K. Hooshyari, M. Javanbakht, L. Naji and M. Enhessari, *J. Membr. Sci.*, 2014, **454**, 74–81.
14 R. Padmavathi and D. Sangeetha, *Ionics*, 2013, **19**, 1423–1436.
15 Z. Jiang, X. Zhao and A. Manthiram, *Int. J. Hydrogen Energy*, 2013, **38**, 5875–5884.
16 A. K. Mishra, N. H. Kim, D. Jung and J. H. Lee, *J. Membr. Sci.*, 2014, **458**, 128–135.
17 Q. Xie, Y. Li, X. Chen, J. Hu, L. Li and H. Li, *J. Power Sources*, 2015, **282**, 489–497.
18 S. Molla and V. Compan, *Int. J. Hydrogen Energy*, 2014, **39**, 5121–5136.
19 S. L. Zhong, X. J. Cui, H. L. Cai, T. Z. Fu, C. Zhao and H. Na, *J. Power Sources*, 2007, **164**, 65–72.
20 S. Sasikala, S. Meenakshi, S. D. Bhat and A. K. Sahu, *Electrochim. Acta*, 2014, **135**, 232–241.
21 P. Kalappa and J. H. Lee, *Polym. Int.*, 2007, **56**, 371–375.
22 S. Seetharamana, S. C. Raghub and K. Ansari Mahabadia, *J. Energy Chem.*, 2016, **25**, 77–84.
23 J. M. Song, H. S. Woo, J. Y. Sohn and J. Shin, *J. Ind. Eng. Chem.*, 2016, **36**, 132–138.
24 P. Salarizadeh, M. Javanbakht and S. Pourmahdian, *Solid State Ionics*, 2015, **281**, 12–20.
25 J. Wang, H. Bai, H. Zhang, L. Zhao, H. Chen and Y. Li, *Electrochim. Acta*, 2015, **152**, 443–455.
26 Y. Yin, T. Xu, G. He, Z. Jiang and H. Wu, *J. Power Sources*, 2015, **276**, 271–278.
27 H. Wu, X. Shen, T. Xu, W. Hou and Z. Jiang, *J. Power Sources*, 2012, **213**, 83–92.
28 A. Sivasankaran and D. Sangeetha, *Fuel*, 2015, **159**, 689–696.
29 H. Zhang, T. Zhang, J. Wang, F. Pei, Y. He and J. Liu, *Fuel Cells*, 2013, **13**, 1155–1165.
30 P. Salarizadeh, M. Javanbakht, S. Pourmahdian and H. Beydaghi, *Chem. Eng. J.*, 2016, **299**, 320–331.
31 J. Hou, G. Dong, Y. Ye and V. Chen, *J. Membr. Sci.*, 2014, **452**, 229–240.
32 J. Hou, G. Dong, B. Luu, R. G. Sengpiel, Y. Ye, M. Wessling and V. Chen, *Bioresour. Technol.*, 2014, **169**, 475–483.
33 S. Molla and V. Compan, *J. Membr. Sci.*, 2015, **492**, 123–136.
34 J. Zhao, M. Milanova, M. M. C. G. Warmoeskerken and V. Dutschk, *Colloids Surf., A*, 2012, **413**, 273–279.
35 N. Majoul, S. Aouida and B. Bessais, *Appl. Surf. Sci.*, 2015, **331**, 388–391.
36 P. Salarizadeh, M. Javanbakht and M. Abdollahi, *Iran. Polym. J.*, 2012, **21**, 661–668.
37 C. Wang, H. Mao, C. Wang and S. Fu, *Ind. Eng. Chem. Res.*, 2011, **50**, 11930–11934.
38 H. Wang, M. Peng, J. Zheng and P. Li, *J. Colloid Interface Sci.*, 2008, **326**, 151–157.
39 I. Brnardic, M. Huskic, P. Umek and T. H. Grguric, *Ceram. Int.*, 2013, **39**, 9459–9464.
40 R. S. Malik, P. Verma and V. Choudhary, *Electrochim. Acta*, 2015, **152**, 352–359.
41 M. Kim, L. Lee, Y. Jung and S. Kim, *J. Nanosci. Nanotechnol.*, 2013, **13**, 7865–7869.
42 R. Vinodh, M. Purushothaman and D. Sangeetha, *Int. J. Hydrogen Energy*, 2011, **36**, 7291–7302.
43 C. Del Rio, E. Morales and P. G. Escribano, *Int. J. Hydrogen Energy*, 2014, **39**, 5326–5337.
44 S. Neelakandan, P. Kanagaraj, A. Nagendran, D. Rana, A. Muthumeenal and T. Matsuura, *Renewable Energy*, 2015, **78**, 306–313.
45 H. Zhang, C. Ma, J. Wang, X. Wang, H. Bai and J. Liu, *Int. J. Hydrogen Energy*, 2014, **39**, 974–986.
46 G. Rambabu and S. D. But, *Chem. Eng. J.*, 2014, **243**, 517–525.
47 A. Shirdast, A. Sharif and M. Abdollahi, *J. Power Sources*, 2016, **306**, 541–551.
48 T. Fu, J. Wang, J. Ni, Z. Cui, S. Zhong, C. Zhao, H. Na and W. Xing, *Solid State Ionics*, 2008, **179**, 2265–2273.
49 M. J. Kayser, M. X. Reinholdt and S. Kaliaguine, *J. Phys. Chem. B*, 2010, **114**, 8387–8395.
50 S. Feng, Y. Shang, G. Liu, W. Dong, X. Xie, J. Xu and V. K. Mathur, *J. Power Sources*, 2010, **195**, 6450–6458.
51 Y. Li, Q. T. Nguyen, P. Schaetzel, C. Lixon-Buquet, L. Colasse, V. Ratieuville and S. Marais, *Electrochim. Acta*, 2013, **111**, 419–433.
52 C. Y. Huang, J. S. Lin, W. H. Pan, C. M. Shih, Y. L. Liu and S. J. Lue, *J. Power Sources*, 2016, **303**, 267–277.
53 J. Park and D. Kim, *Int. J. Hydrogen Energy*, 2014, **39**, 1063–1070.
54 R. Gosalawit, S. Chirachanchai, S. Shishatskiy and S. P. Nunes, *J. Membr. Sci.*, 2008, **323**, 337–346.
55 Z. Gaowen and Z. Zhentao, *J. Membr. Sci.*, 2005, **261**, 107–113.
56 E. B. Cho, D. X. Luu and D. Kim, *J. Membr. Sci.*, 2010, **351**, 58–64.
57 D. Marani, A. Epifanio, E. Traversa, M. Miyayama and S. Licoccia, *Chem. Mater.*, 2010, **22**, 1126–1133.
58 M. M. Hasani-Sadrabadi, S. H. Emami, R. Ghaffarian and H. Moaddel, *Energy Fuels*, 2008, **22**, 2539–2542.
59 H. Wu, Y. Cao, Z. Li, G. He and Z. Jiang, *J. Power Sources*, 2015, **273**, 544–553.
60 Y. He, J. Wang, H. Zhang, T. Zhang, B. Zhang, S. Cao and J. Liu, *J. Mater. Chem. A*, 2014, **2**, 9548–9558.
61 R. P. Pandey, A. K. Thakur and V. K. Shahi, *ACS Appl. Mater. Interfaces*, 2014, **6**, 16993–17002.
62 S. Gahlot, P. P. Sharma, V. Kulshrestha and P. K. Jha, *ACS Appl. Mater. Interfaces*, 2014, **6**, 5595–5601.
63 J. Park, S. Y. Han and D. Kim, *Int. J. Hydrogen Energy*, 2015, **40**, 8160–8171.